https://doi.org/10.30799/jnst.310.20060304 J. Nanosci. Tech. - Volume 6 Issue 3 (2020) 911–914

Share Your Innovations through JACS Directory

Journal of Nanoscience and Technology

Visit Journal at https://www.jacsdirectory.com/jnst

ISSN: 2455-0191

Enhanced Acidic Hydrogen Evolution on TiO_2-Doped Gadolinium Electrocatalysts

Mohammed Alsawat*

Department of Chemistry, Faculty of Science, Taif University, Taif, Saudi Arabia.

ARTICLEDETAILS

Article history:
Received 13 September 2020
Accepted 20 September 2020
Available online 26 September 2020

Keywords:
Gadolinium-Doped TiO_2 NPs
Electrocatalysis
Hydrogen Evolution Reaction
Acidic Electrolyte

ABSTRACT

Gadolinium-doped TiO_2 NPs, namely TiO_2-$Gd_{1.0}$ and TiO_2-$Gd_{6.0}$ have been synthesized using two different atomic concentrations of gadolinium(III) nitrate hexahydrate in presence of titanium(IV) *tert*-butoxide as a titanium precursor and dimethyl sulfoxide as a solvent. The structure and morphology of these NPs have been characterized by Fourier transform infrared spectroscopy (FTIR), thermogravimetric-differential thermal analysis (TGA-DTA), X-ray diffraction (XRD), scanning electron microscopy (SEM), and transmission electron microscopy (TEM). The two synthesized TiO_2-$Gd_{1.0}$ and TiO_2-$Gd_{6.0}$ were tested as electrocatalysts for hydrogen evolution reaction (HER) in an acidic electrolyte (0.5 M H_2SO_4) based on linear sweep voltammetry (LSV) measurements. LSV data were fitted to Tafel equation and the various electrochemical parameters describing the HER kinetics were evaluated and discussed. Results demonstrate that the kinetics of the HER on the surface of TiO_2 NPs significantly enhanced upon doping it with Gd^{3+}, proportionally to the atomic concentration of the Gd^{3+} cations in the TiO_2 NPs.

1. Introduction

Water electrolysis is one of the key approaches used for producing CO_2-free hydrogen. However, this electrochemical method involves a high electricity to smash the chemical links in the water molecule between oxygen and hydrogen, which makes it financially costly [1]. In order to minimize this expense, the process is conducted at elevated temperatures, but increasing the temperature is a further kind of energy consumption, so the researchers used catalysts to efficiently accelerate the reaction at room temperature to achieve a high hydrogen yield at lower costs [2].

Literature reported a huge number of newly synthesized materials for the electrochemical production of hydrogen from various aqueous media with a wide range of pH [3]. Most of them, particularly the most efficient ones, are unstable and expensive. Literature also revealed an intense shortage of information on TiO_2 NPs-doped rare earth ions in electrocatalysis applications [4,5]. The Fermi level of TiO_2 is higher than that of gadolinium and accordingly the excited electrons of the TiO_2 are transferred to gadolinium deposited on its surface. Therefore, the probability of electron-hole recombination are limited leading to efficient separation of charges [6]. Moreover, rare earth elements featuring 4f electronic configuration and hence are very suitable dopants for adjusting properties of TiO_2. Among the rare earth elements, neodymium and gadolinium are commonly used dopants for different applications [7]. Recently, workers including my group studied the role of palladium and europium on TiO_2 performance and they have obtained a positive effect towards the catalysis of the hydrogen energy reaction (HER) [5-8].

This work aims to generate a hydrogen gas with high efficiency at room temperatures using safe, inexpensive, and easily prepared new materials. In this context, two TiO_2 NPs-x% doped Gd^{3+}, (x = 1.0 and 6.0 wt%) were synthesized and fully characterized, and employed here as electrocatalysts for the hydrogen evolution reaction (HER) as literature revealed no articles on the kinetics of the HER on these materials. The electrocatalytic activity of such two nanocomposites toward the HER was investigated in an aqueous (deaerated) H_2SO_4 solution (0.5 M) employing LSV technique. Measurements were conducted in a comparison with bare GC and TiO_2 NPs/GC electrodes.

2. Experimental Methods

2.1 Synthesis of Gd^{3+}-Doped TiO_2 NPs

The TiO_2-$Gd_{1.0}$ and TiO_2-$Gd_{6.0}$ NPs were prepared following a previously reported method [9-14]. Briefly, titanium (IV) *tert*-butoxide (5.0 mL) was added to gadolinium(II) nitrate hexahydrate with two different atomic concentrations (1.0. and 6.0%) in DMSO (50 mL). The mixed solution was reflexed at 190 °C for 2 h. The obtained precipitate was collected by centrifuge (6000 rpm), washed several times with ethanol/acetone (2:1), and dried. Then, the obtained powders were calcinated at 400 °C for 2 h.

2.2 Characterizations of TiO_2-$Gd_{1.0}$ and TiO_2-$Gd_{6.0}$ NPs

The FT-IR spectra were recorded using Alpha-Atunated FT-IR spectrophotometer, Bruker in the range of 400–4000 cm^{-1}. X-ray powder diffraction (XRD) has been carried out using a D8 Advance (Bruker, USA) X-Ray diffractometer with CuKα operated at 40 kV and 40 mA. The program X'pert HighScore Plus (PANalytical, The Netherlands) was used to carry out the XRD pattern fitting of TiO_2, TiO_2-$Gd_{1.0}$ and TiO_2-$Gd_{6.0}$ NPs [15]. This gives peak position (2θ), intensity (I), relative intensity (IR), half width (HW), etc. The Scherrer equation was used to estimate the crystallite size for each of the diffraction peaks, where the crystallite size was calculated as $D = k\lambda/HW.\cos\theta$ [16]. The constant k was taken equal to 0.9 and the used wavelength $k_{\alpha 1} = 1.54056$ Å then the average values were calculated. The least squares refinement method of Holland and Redfern was employed to retrieve unit cell constants from diffraction peak position [17]. The morphology of the prepared samples was investigated using scanning electron microscopy (Hitachi S-4700 FE-SEM) equipped with energy dispersive X-ray spectroscopy (EDX) and by using transmission electron microscope (Phillips CM200 TEM) operated at 200 kV. Simultaneous thermogravimetric analysis (TGA) coupled with differential thermal analysis (DTA) measurements were recorded using Shimadzu DTG 60H with system interface device in the atmosphere of nitrogen. The operational range of the instrument was from ambient temperature to 1000 °C at a heating rate of 10 °C min^{-1}.

2.3 Electrochemical Measurements

The working electrode (WE) employed in this work was a glassy carbon (GC) electrode loaded with a specific mass of the tested catalyst powder. The GC-loaded catalyst (WE) was prepared as follows. A mirror-like GC working electrode surface is first obtained *via* polishing with 0.3 µm alumina powder followed by 0.05 µm. It was then subjected to 20 minutes of ultrasonic washing using double-distilled water, and eventually dried into the air. Then, an aqueous dispersion (ink) of the catalyst (20 µL, 1.0

*Corresponding Author:mosawat@tu.edu.sa(Mohammed Alsawat)

https://doi.org/10.30799/jnst.310.20060304

mg/mL) was dropped onto the freshly polished, mirror-like, GC electrode, yielding a catalyst with a loading density of about 0.28 μgcm^{-2}.

The HER catalytic performance of the prepared nanocomposites was evaluated using a d.c. linear polarization technique, namely linear sweep voltammetry (LSV). In order to conduct an LSV experiment, the WE first cathodically (linearly) scanned with a potential sweep rate of 5.0 mVs^{-1} starting from the corrosion potential (E_{corr}).

In traditional electrochemical standard cell, electrochemical measurements have been conducted using Ag/AgCl and a long spiral Pt wires as the reference and counter electrodes. Potentials were measured against Ag/AgCl reference electrode, and then converted to the reversible electrode hydrogen (RHE) scale using the formula,

$$E_{RHE} = E_{Ag/AgCl} + E^{\circ}_{Ag/AgCl} + 0.059 \times pH$$

where, pH = 0 and $E^{\circ}_{Ag/AgCl}$= 0.2046 V (25 °C). Measurements were performed at room temperature in a volume cell of 200 mL. An Autolab, Potentiostat/Galvanostat (PGSTAT30), was connected to the electrochemical cell to apply the LSV technique on the GC-catalyst/electrolyte interface. The test electrolyte was an aqueous solution of H_2SO_4 (0.5 M). Prior to use, the test solution was deaerated through 30 minutes of purging with Ar. The argon blanket has been kept on the solution during the entire experiment, to prevent convection effects. Repeating at least three measurements verified the strong reproducibility of the LSV and EIS findings. The average and standard deviation of the results have been estimated and reported.

3. Results and Discussion

3.1 Structural Analysis

The reaction of titanium(IV) *tert*-butoxide in presence of gadolinium(III) nitrate hexahydrate in boiling DMSO as solvent and oxidizing agent [9] produces the Gd^{3+}-$Ti(OH)_4$ monomer. These hydroxide monomers were then reacted with the dimethyl sulfoxonium cation [18], which evolved from the degradation of DMSO molecules deposited at the surfaces of Gd^{3+}-doped TiO_2 NPs. The formation of $Ti(OH)_4$ slows the growth of these NPs and prevents their agglomeration [19]. The FT-IR spectra of TiO_2-$Gd_{1.0}$ NPs before and after the calcination process are shown in Fig. 1.

Before annealing, the FT-IR spectrum of the synthesized precursor Gd^{3+}-doped TiO_2 shows vibration bands in the region of 1000–1250 cm^{-1}, indicating the presence of *tert*-butoxy groups. Other two peaks at 1584 and 3383 cm^{-1} can be attributed to δH_2O bending and hydroxyl groups [20]. After annealing, the aforementioned peaks were not detected confirming the remove of all organic compounds from the samples by calcination.

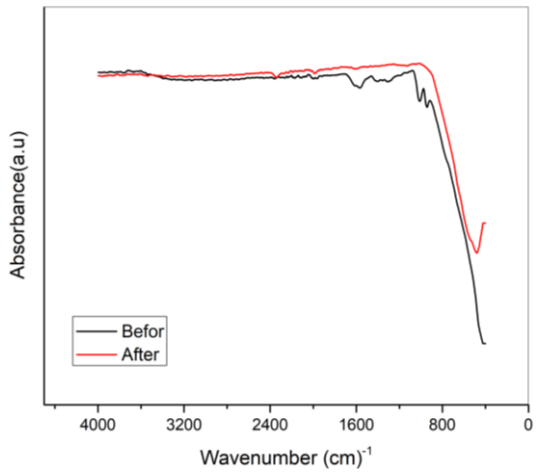

Fig. 1 FT-IR spectra of TiO_2-$Gd_{1.0}$ NPs before (Black) and after calcination (Red)

The thermal decomposition of TiO_2-$Gd_{1.0}$ NPs before and after the calcination process is measured by simultaneous TGA-DTG-DTA in the range of 25-1000 °C. Before calcination, The TGA curve (Fig. 2a) displays three main steps. The first endothermic peak at 110 °C could be ascribed to the dehydration of adsorbed water molecules on the surface of TiO_2-$Gd_{1.0}$ NPs as well as the volatilization of the remaining organic solvent. The other two exothermic peaks at 250 and 510 °C were assigned to the degradation of organic moieties [21,22]. After calcination, no TGA weight losses are detected (Fig. 2b), confirming the high thermal stability of the prepared TiO_2-$Gd_{1.0}$ NPs.

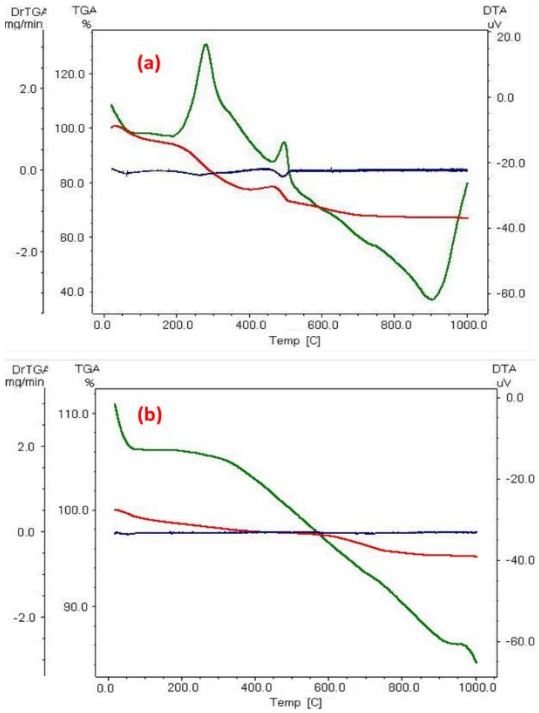

Fig. 2 TGA-DTG-DTA curves of TiO_2-$Gd_{1.0}$ NPs recorded in the range of 25-1000 °C a) before and b) after calcination

The XRD patterns of TiO_2, TiO_2-$Gd_{1.0}$ and TiO_2-$Gd_{6.0}$ NPs fitted using X'pert HighScore Plus (Fig. 3). The XRD pattern of TiO_2 shows peaks at 2θ = 25.3°, 37.9°, 47.9°, 55°, 62.7°, 68.9°, and 75.2°, which correspond to the anatase crystallographic phase of TiO_2 [23-25]. The XRD patterns of TiO_2-$Gd_{1.0}$ and TiO_2-$Gd_{6.0}$ NPs show the same peaks positions with slight increment in the peaks' intensity which can be attributed to higher crystallinity. The anatase phase with the tetragonal lattice was refined in the space group $I4_1/amdI4_1/amd$ [26] and dominated the composition of all TiO_2 samples. Table 1 shows the cell parameters and crystallite size of TiO_2, TiO_2-$Gd_{1.0}$, and TiO_2-$Gd_{6.0}$. The cell parameter *a* increases, which is due to the substitution of the Ti^{4+} by Gd^{3+} ions inside the TiO_2 lattice [27].

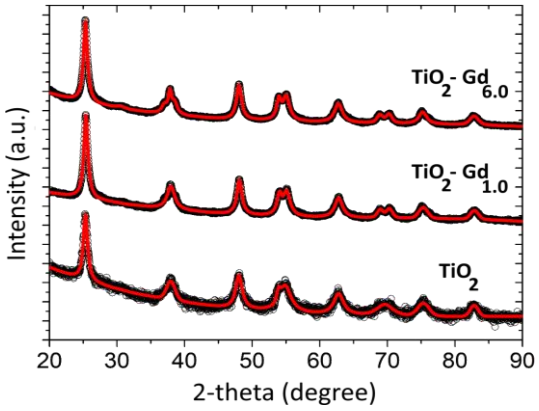

Fig. 3 XRD patterns where the black circles are the observed data and the red solid line is the calculated profile of TiO_2, TiO_2-$Gd_{1.0}$ and TiO_2-$Gd_{6.0}$ NPs

Table 1 The cell parameters and crystallite size of TiO_2, TiO_2-$Gd_{1.0}$, and TiO_2-$Gd_{6.0}$

NPs	a (Å)	c (Å)	D (nm)
TiO_2	3.781(2)	9.414(6)	8(3)
TiO_2-$Gd_{1.0}$	3.785(2)	9.487(6)	10(3)
TiO_2-$Gd_{6.0}$	3.789(2)	9.488(6)	10(3)

In order to investigate the morphology of the nanocomposites, SEM equipped with EDX was used. Fig. 4a shows the SEM of TiO_2-$Gd_{1.0}$ NPs as a representative example of Gd^{3+}-doped TiO_2 NPs. It shows the presence of spherical particles ($Gd_{1.0}$) deposited on the surface of TiO_2 NPs. The composition of the nanocomposite was confirmed by the EDX, which shows the presence of Ti^{4+} and Gd^{3+} ions (Fig. 4b).

The morphology of TiO_2-$Gd_{1.0}$ was further investigated by transmission electron microscopy. It can be seen from the TEM images (Fig. 5) that the TiO_2-$Gd_{1.0}$ has a uniform size in quasi-spherical and cubic type particles. Upon doping TiO_2 with different concentrations of Gd^{3+}, the average size was slightly increased.

https://doi.org/10.30799/jnst.310.20060304

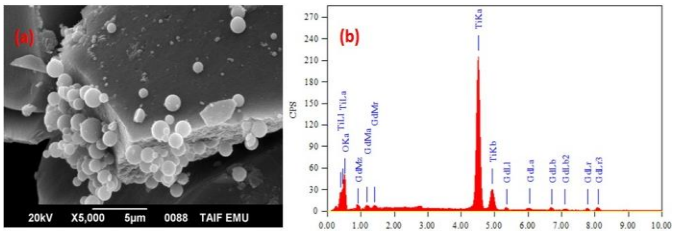

Fig. 4 (a) SEM image and (b) EDX analysis of TiO_2-$Gd_{1.0}$ NPs

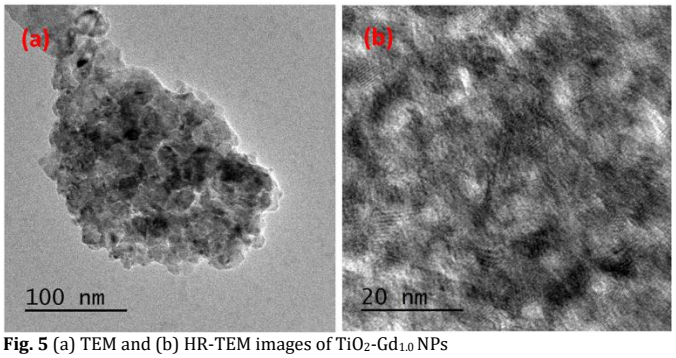

Fig. 5 (a) TEM and (b) HR-TEM images of TiO_2-$Gd_{1.0}$ NPs

3.2 HER Studies (LSV Measurements)

Fig. 6a represents the linear sweep voltammetry (LSV) curves, conducted at room temperature in 0.5 M H_2SO_4 solution at a potential scan rate of 5.0 mVs^{-1}, for the two synthesized catalysts, namely $Gd_{1.0}/TiO_2$ and $Gd_{6.0}/TiO_2$ in a comparison with bare GCE and TiO_2/GCE. The cathodic polarization data of Fig. 6a were fitted to Tafel equation, yielding the Tafel plots depicted in Fig. 6b, to extract the various electrochemical parameters of the HER associated with such cathodic polarization measurements.

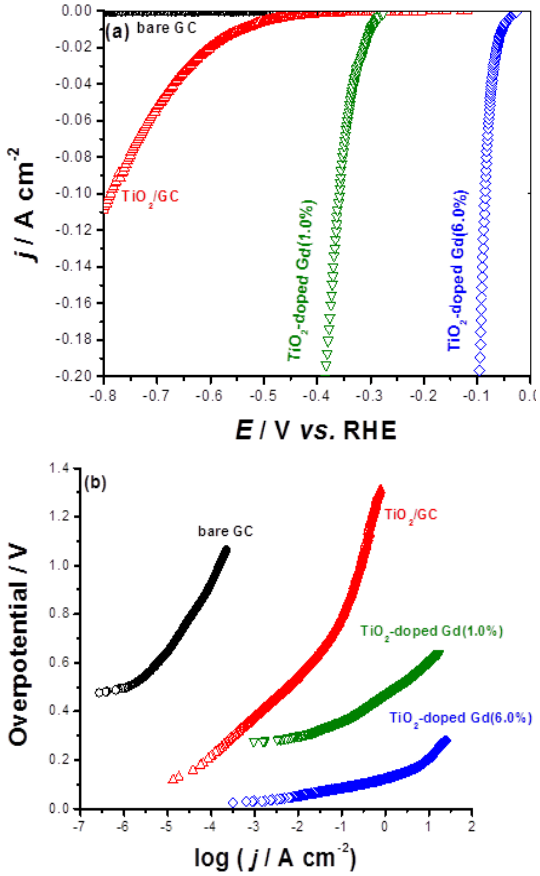

Fig. 6 LSV curves (a) and the corresponding Tafel plots (b) for the studied catalysts. Measurements were conducted in deaerated 0.5 M H_2SO_4 solution at a scan rate of 5.0 mVs^{-1} at room temperature

These HER electrochemical parameters, which include the exchange current density (j_o), Tafel slope (β_c), and the overpotential (η_{10}) the catalyst must acquire to generate a current density of 10 $mAcm^{-2}$, will be used to fully describe the kinetics of the HER on the surface of the tested catalysts. These parameters are listed in Table 2.

Table 2 Mean value (standard deviation) of the electrochemical HER kinetic parameters on studied electrocatalysts. Measurements were conducted at room temperature in deaerated 0.5 M H_2SO_4 solution in a comparison with bare GCE and TiO_2/GCE

Tested cathode	Onset potential (E_{HER}, mV *vs.* RHE)	Tafel slope (β_c, $mVdec^{-1}$)	Exchange current density (j_o, $mAcm^{-2}$)	Overpotential at j = 10 $mAcm^{-2}$ (η_{10}, mV)
bare GCE	-500(12)	-266(2.8)	$3.98(0.09) \times 10^{-5}$	---
TiO_2 NPs	-350(6)	-168(2)	$5.5(0.12) \times 10^{-3}$	540(6.8)
$Gd_{1.0}/TiO_2$	-95(2.1)	-118(1.6)	$12(0.2) \times 10^{-2}$	290 (4.2)
$Gd_{6.0}/TiO_2$	-40(0.9)	-33(0.7)	$25(0.5) \times 10^{-2}$	55 (1.1)

Being a well-known poor catalyst, the GCE is expected to exhibit very low catalytic activity for the HER. This is evidenced here from its highly negative onset potential for the HER, E_{HER} (-500 mV *vs.* RHE), beyond which very little cathodic currents were generated, as shown in Fig. 6a, Curve 1. Compared to the bare GCE, the studied supporting material in this work, namely TiO_2 NPs (an n-type semiconductor material [28]) showed a considerable catalytic activity for the HER even in the dark [5,10,14], Curve 2. It recorded lower (less negative, i.e., more nodic) E_{HER} value (-350 mV *vs.* RHE) with larger cathodic currents produced beyond it. The considerable HER catalytic response of TiO_2 NPs can be attributed to the fact that the semiconductor electrodes of n-type can produce significant cathodic currents under dark conditions [29, 30].

The catalytic performance of TiO_2 NPs towards the HER is significantly improved upon doping it with 1.0 and 6.0% Gd^{3+}, Curves 3 and 4. This improvement in the HER catalytic performance of TiO_2-doped Gd^{3+} is enhanced with the Gd^{3+} doping percentage. This is clear from Table 2. The E_{HER} value has markedly reduced from -350 mV vs. RHE for pure TiO_2 to -95 mV *vs.* RHE and -40 mV *vs.* RHE for TiO_2-doped 1.0% Gd^{3+} and TiO_2-doped 6.0% Gd^{3+}, respectively. The overpotential (η_{10}) acquired by an electrocatalyst to deliver a current density of 10 $mAcm^{-2}$ is another important electrochemical parameter controlling the electrocatalyst's performance [31]. The lower, i.e., less negative (more anodic), the η_{10} value the higher is its catalytic activity. From Table 2, the η_{10} value decreases following the sequence: TiO_2 (540 mV) <<TiO_2-doped 1.0% Gd^{3+} (290 mV) < TiO_2-doped 6.0% Gd^{3+} (55 mV). These results present TiO_2-doped 6.0% Gd^{3+} as the best performing electrocatalyst.

Such reduced values of E_{HER} and η_{10} favor H_2 generation at lower overpotentials resulting in higher j_o values. Data in Table 2 confirmed that; the value of j_o is considerably increased (~22 times) from 5.5×10^{-3} $mAcm^{-2}$ for TiO_2 alone (i.e., without doping) to 12×10^{-2} mA for TiO_2-doped 1.0% Gd^{3+} catalyst. This TiO_2-doped 1.0% Gd^{3+} catalyst's j_o value is doubled when Gd^{3+} percentage doping is increased from 1.0 to 6.0%.

The Tafel slope is another HER electrochemical kinetic parameter essentially employed to evaluate and compare the HER catalytic performance of the tested catalysts. Lower Tafel slopes reveal accelerated HER kinetics [32].

Classical theory [33-35] has shown that, in acidic aqueous media, the Tafel slope values associated with the HER mechanisms proceeded by Volmer (Eq.1), Heyrovsky (Eq.2) and Tafel (Eq.3) were calculated to be approximately 120 $mVdec^{-1}$, 40 $mVdec^{-1}$ and 30 $mVdec^{-1}$.

$$H_3O^+ + e^- + S \rightarrow SH_{ads} + H_2O \quad \text{(Volmer step)} \quad (1)$$

$$b = \frac{2.34RT}{\alpha F} \cong 120 \text{ mV/dec}$$

$$H_3O^+ + e^- + SH_{ads} \rightarrow S + H_2O + H_2 \quad \text{(Heyrovsky)} \quad (2)$$

$$b = \frac{2.34RT}{2F} \cong 40 \text{ mV/dec}$$

$$SH_{ads} + SH_{ads} \rightarrow 2S + H_2 \quad \text{(Tafel step)} \quad (3)$$

$$b = \frac{2.34RT}{(1+\alpha)F} \cong 30 \text{ mV/dec}$$

where the SH_{ads} denote the hydrogen atom adsorbed chemically on an active catalytic site (S). The pronounced diminish in the Tafel slope value from 168 $mVdec^{-1}$ for the TiO_2/GCE catalyst to 118 $mVdec^{-1}$ for TiO_2-doped 1.0% Gd^{3+} catalyst and 33 $mVdec^{-1}$ for TiO_2-doped 6.0% Gd^{3+} catalyst ranks the kinetics of the HER over studied catalysts as: TiO_2/GCE <TiO_2-doped 1.0% Gd^{3+}<TiO_2-doped 6.0% Gd^{3+}. These results confirm the catalytic impact of the doped Gd^{3+} on the HER kinetics on TiO_2 NPs.

The best catalyst here, namely TiO_2-doped 6.0% Gd^{3+} recorded a small Tafel slope value of 33 $mVdec^{-1}$, which is close to that reported in the literature as well as in our lab [36, 37] for the commercial Pt/C catalyst (~30 $mVdec^{-1}$) under the same operating conditions. These results present Volmer-Tafel steps, Eqs.(1) and (3), with the recombination (Tafel) step

https://doi.org/10.30799/jnst.310.20060304

being the rate limiting [35], as the possible mechanism for the HER over the tested catalysts.

The tight chemical coupling between the supporting material, namely TiO_2 NPs and the doped Gd NPs may be one of the major reasons behind the high HER catalytic performance of the two studied TiO_2-doped Gd^{3+} catalysts. This high chemical interaction results in the formation of highly sparse (aggregation-free) metal NPs selectively growing on the surface of TiO_2. The existence of such doped Gd NPs, whose population is logically enhanced with its doping percentage, in the TiO_2 crystal lattices expected to provide the HER with abundant active catalytic sites. It is believed that each supported (even doped) metallic NP can be viewed as a nanoelectrode or even a proton reducing nanocathode [36]. Another explanation for its increased catalytic activity against the HER may be the large electrochemical surface area of such catalysts caused by the high specific surface area of the supporting material (TiO_2 NPs, 136.87 m^2/g [M4]) itself. In fact, high-specific surface area substrates allow a good dispersion of the supported NPs with significantly reduced size. This, in turn, boosts the exposure of more active HER sites [36].

4. Conclusion

Gadolinium-doped TiO_2 NPs, namely TiO_2-$Gd_{1.0}$ and TiO_2-$Gd_{6.0}$ were fabricated and fully characterized using FTIR, TGA-DTA, XRD, SEM and TEM. XRD investigations showed that Ti^{4+} was properly substituted by Gd^{3+} in the TiO_2 host lattice. The two synthesized TiO_2 NPs-doped Gd^{3+} exhibited remarkable catalytic activity towards the HER in sulphuric acid solution (0.5 M). The catalytic performance was found to improve with increase in doped Gd^{3+} content in the nanocomposite. This is evidenced from the two essential HER electrochemical kinetic parameters, namely j_o and η_{10} employed to evaluate and compare the HER catalytic activity of the tested electrocatalysts. The TiO_2-$Gd_{6.0}$ catalyst consumed an overpotential of η_{10} = 55 mV to deliver a current density of 10 $mAcm^{-2}$. On the other hand, the TiO_2-$Gd_{1.0}$ acquired much higher overpotential (η_{10} = 290 mV) to achieve the same current. Also, the TiO_2-$Gd_{6.0}$ catalyst recorded an j_o value (0.25 $mAcm^{-2}$) as twice as that calculated for the TiO_2-$Gd_{1.0}$, 0.12 $mAcm^{-2}$. These findings indicated that TiO_2-$Gd_{6.0}$ catalyst is more catalytically active than the TiO_2-$Gd_{1.0}$ catalyst.

References

[1] D. Pletcher, X. Li, Prospects for alkaline zero gap water electrolysers for hydrogen production, Int. J. Hydrogen Energ. 36 (2011) 15089-15104.

[2] T. Kato, M. Kubota, N. Kobayashi, Y. Suzuoki, Y, Effective utilization of by-product oxygen from electrolysis hydrogen production, Energy 30 (2005) 2580-2595.

[3] A. Eftekhari, Electrocatalysts for hydrogen evolution reaction, Int. J. Hydrogen Energ. 42 (2017) 11053-11077.

[4] X. Kang, S. Liu, Z. Dai, Y. He, X. Song, Z. Tan, Titanium dioxide: From engineering to applications, Catalysts 9 (2019) 191-223.

[5] M.M. Ibrahim, A. Mezni, M. Alsawat, T. Kumeria, M.R. Das, et al., Enhanced hydrogen evolution reaction on highly stable titania-supported PdO and Eu_2O_3 nanocomposites in a strong alkaline solution, Int. J. Energy Res. 43 (2019) 5367-5383.

[6] M. Ye, J. Gong, Y. Lai, C. Lin, Z. Lin, High-efficiency photoelectrocatalytic hydrogen generation enabled by palladium quantum dots-sensitized TiO_2 nanotube arrays, J. Am. Chem. Soc. 134 (2012) 15720−15723.

[7] S. Amiri, H. Shokrollahi, Magnetic and structural properties of RE doped Co-ferrite (RE, Nd, Eu, and Gd) nano-particles synthesized by co-precipitation, J. Magn. Magn. Mater. 345 (2013) 18-23.

[8] N.R. Khalid, M. Liaqat, M.B. Tahir, G. Nabi, T. Iqbal, N.A. Niaz, The role of graphene and europium on TiO_2 performance for photocatalytic hydrogen evolution, Ceram. Int. 44 (2018) 546−549.

[9] A. Mezni, N.B. Saber, M.M. Ibrahim, M. El-Kemary, A. Aldalbahi, et al., Facile synthesis of highly thermally stable TiO_2 photocatalysts, New J. Chem. 41 (2017) 5021-5027.

[10] A. Mezni, M.M. Ibrahim, M. El-Kemary, A.A. Shaltout, N.Y. Mostafa, et al., Cathodically activated Au/TiO_2 nanocomposite synthesized by a new facile solvothermal method: An efficient electrocatalyst with Pt-like activity for hydrogen generation, Electrochim. Acta 290 (2018) 404-418.

[11] A. Mezni, N.B. Saber, M.M. Ibrahim, N. Hamdaoui, A. Alrooqi, A. Mlayah, Photocatalytic activity of hybrid gold-titania nanocomposites, Mater. Chem. Phys. 221 (2019) 118-124 (IF = 2.210).

[12] M.M. Ibrahim, A. Mezni, H.S. El-Sheshtawy, A.A. Abu Zaid, M. Alsawat, et al., Direct Z-scheme of Cu_2O/TiO_2 enhanced self-cleaning, antibacterial activity, and UV protection of cotton fiber under sunlight, Appl. Surf. Sci. 479 (2019) 953-962.

[13] A. Mezni, N. Ben Saber, A. Bukhari, M.M. Ibrahim, H. Al-Talhi, et al., Plasmonic hybrid platinum-titania nanocomposites as highly active photocatalysts: self-cleaning of cotton fiber under solar light, J. Mater. Res. Technol. 9 (2020) 1447-1456.

[14] M.M. Ibrahim, A. Mezni, M. Alsawat, T. Kumeria, A. Alrooqi, et al., Crystalline ZnO and ZnO/TiO_2 nanoparticles derived from tert-butyl N-(2 mercaptoethyl)carbamatozinc(II) chelate: Electrocatalytic studies for H_2 generation in alkaline electrolytes, Int. J. Energy Res. 44 (2020) 6725-6744.

[15] T.Degen, M. Sadki, E. Bron, U. König, G. Nénert, The HighScore suite, Powder Diffr. 29(S2) (2014) S13-S18.

[16] A.L. Patterson, The Scherrer formula for X-ray particle size determination, Phys. Rev. 56 (1939) 978-982.

[17] T. Holland, S. Redfern, Unit cell refinement from powder diffraction data: the use of regression diagnostics, Mineralog. Magaz. 61 (1997) 65-77.

[18] D. Head, G. Mc Carty, The thermal decomposition of DMSO, Tetrahedron Lett. 16 (1973) 1405-1408.

[19] A. Mezni, I. Balti, A. Mlayah, N. Jouini, L.S. Smiri, Hybrid Au–Fe_3O_4 nanoparticles: Plasmonic, surface enhanced raman scattering, and phase transition properties, J. Phys. Chem. C 117 (2013) 16166-16174.

[20] A. Mezni, F. Kouki, S. Romdhane, B. Fonrose, S. Joulie, et al., Facile synthesis of ZnO nanocrystals in polyol, Mat. Lett. 86 (2012) 153-156.

[21] W. Que, Y. Zhou, Y.L. Lam, Y.C. Chan, C.H. Kam, Preparation and characterizations of TiO_2/organically modified silane composite materials produced by the sol-gel method, J. Sol–Gel Sci. Technol. 20 (2001) 187-195.

[22] B.L. Wang, L.L. Hu, Effect of water content in sol on optical properties of hybrid sol–gel derived TiO_2/SiO_2/ormosil film, Mater. Chem. Phys. 89 (2005) 417–422.

[23] ICDD PDF 2, Database Sets 1–45, The International Centre for Diffraction Data: PA, USA, 1995.

[24] ICSD database, Version 2005-1; Fachinformationszentrum Karlsruhe, Germany, and the U.S. Department of Commerce, USA, 2005.

[25] L. Lutterotti, P. Scardi, Simultaneous structure and size-strain refinement by the Rietveld method, J. Appl. Crystallogr. 23 (1990) 246-252.

[26] L. Lutterotti, Total pattern fitting for the combined size–strain–stress–texture determination in thin film diffraction, Nucl. Instrum. Methods Phys. Res. B 286 (2010) 334-340.

[27] L. Vegard, Die Konstitution der Mischkristalle und die Raumfüllung der Atome, Z. Physik 5 (1921) 17-26.

[28] A. Kubiak, K. Siwinska-Ciesielczyk, T. Jesionowski, Titania-based hybrid materials with ZnO, ZrO_2 and MoS_2: A review, Materials 11 (2018) 2295:1-52.

[29] K.L. Hardee, A.J. Bard, Semiconductor electrodes: X. Photoelectrochemical behavior of several polycrystalline metal oxide electrodes in aqueous solutions, J. Electrochem. Soc. 77 (1977) 215-224.

[30] A.W. Bott, Electrochemistry of semiconductors, Curr. Sep. 17 (1998) 87-91.

[31] A. Eftekhari, Electrocatalysts for hydrogen evolution reaction, Int. J. Hydrogen Energ. 42 (2017) 11053-11077.

[32] T. Shinagawa, A.T. Garcia-Esparza, K. Takanabe, Insight on Tafel slopes from a microkinetic analysis of aqueous electrocatalysis for energy conversion, Sci. Rep. 5 (2015) 13801:1-21.

[33] Y. Sun, C. Liu, D.C. Grauer, J. Yano, J.R. Long, P. Yang, C.J. Chang, Electrodeposited cobalt-sulfide catalyst for electrochemical and photoelectrochemical hydrogen generation from water, J. Am. Chem. Soc. 135 (2013) 17699-17702.

[34] P.D. Tran, M. Nguyen, S.S. Pramana, A. Bhattacharjee, S.Y. Chiam, et al., Copper molybdenum sulfide: a new efficient electrocatalyst for hydrogen production from water, Energy Environ. Sci. 5 (2012) 8912-8916.

[35] J.G.N. Thomas, Kinetics of electrolytic hydrogen evolution and the adsorption of hydrogen by metals, Trans. Faraday Soc. 57 (1961) 1603-1611.

[36] G. Darabdhara, M.A. Amin, G.A.M. Mersal, E.M. Ahmed, M.R. Das, et al., Reduced graphene oxide nanosheets decorated with Au, Pd and Au–Pd bimetallic nanoparticles as highly efficient catalysts for electrochemical hydrogen generation, J. Mater. Chem. A 3 (2015) 20254-20266.

[37] G. Darabdhara, M.R. Das, M.A. Amin, G.A.M. Mersal, N.Y.Mostafa, et al., Au single bond Ni alloy nanoparticles supported on reduced graphene oxide as highly efficient electrocatalysts for hydrogen evolution and oxygen reduction reactions, Int. J. Hydrogen Energ. 43 (2018) 1424-1438.

https://doi.org/10.30799/jnst.310.20060304

Cite this Article as: Mohammed Alsawat, Enhanced acidic hydrogen evolution on TiO_2-doped gadolinium electrocatalysts, J. Nanosci. Tech. 6(3) (2020) 911–914.